

Oxygen adsorption and stability of surface oxides on Cu(111): A first-principles investigationAloysius Soon,^{1,*} Mira Todorova,¹ Bernard Delley,² and Catherine Stampfl¹¹*School of Physics, The University of Sydney, Sydney, Australia*²*Paul-Scherrer-Institut (PSI), Villigen, Switzerland*

(Received 19 December 2005; published 28 April 2006)

As a first step towards gaining microscopic understanding of copper-based catalysts, e.g., for the low-temperature water-gas shift reaction and methanol oxidation reactions, we present density-functional theory calculations investigating the chemisorption of oxygen, and the stability of surface oxides on Cu(111). We report atomic geometries, binding energies, and electronic properties for a wide range of oxygen coverages, in addition to the properties of bulk copper oxide. Through calculation of the Gibbs free energy, taking into account the temperature and pressure via the oxygen chemical potential, we obtain the (p, T) phase diagram of O/Cu(111). Our results show that for the conditions typical of technical catalysis the bulk oxide is thermodynamically most stable. If, however, formation of this fully oxidized surface is prevented due to a kinetic hindering, a thin surface-oxide structure is found to be energetically preferred compared to chemisorbed oxygen on the surface, even at very low coverage. Similarly to the late 4d transition metals (Ru, Rh, Pd, Ag), sub-surface oxygen is found to be energetically unfavorable.

DOI: [10.1103/PhysRevB.73.165424](https://doi.org/10.1103/PhysRevB.73.165424)

PACS number(s): 68.43.Bc, 81.65.Mq, 68.47.Gh

I. INTRODUCTION

Acquiring a fundamental understanding of the nature of the interaction between oxygen and metal surfaces is crucial to explain the role of oxygen in a number of important technological processes such as oxidation, corrosion, and heterogeneous catalysis.^{1,2} This knowledge will assist in enhancing the performance of existing catalysts as well as developing new ones. Many current industrial processes are centered on catalytic oxidation reactions. Upon exposure to an oxygen atmosphere, the structures formed on transition metal (TM) surfaces vary from simple adlayers of chemisorbed oxygen to oxygen diffusion into the sub-surface region and the formation of oxides, depending on the partial pressure, temperature, and orientation of the metal surface. Oxidation catalysts can be rather complex, often involving multiple phases and various active sites to fulfill multiple catalytic functions. Hence a careful study of the role of each phase and its specific interaction under working conditions is required to fine-tune the productivity of these catalysts.

In recent years, there has been a great focus on clean energy technology, bringing a renewed interest in the water-gas shift (WGS) reaction in relation to fuel-cell powered vehicles, where hydrogen is obtained via partial oxidation and steam reforming of hydrocarbons and methanol.³ Copper-based catalysts are well known to be active for methanol synthesis, partial oxidation of methanol and the WGS reaction. The active site, the role of support oxides, and each detailed reaction mechanism are still the focus of considerable controversy, even though a great deal of effort has gone into seeking consensus by conducting *in situ* experiments, in the hope of bridging the “pressure” and “materials” gap.

The O/Cu(111) system has been investigated both theoretically⁴ and experimentally.^{5–15} From these studies, there seems to be a consensus on some aspects of the adsorption behavior of oxygen on Cu(111) under ultra high vacuum (UHV) conditions. For exposures of less than 10^4 L, a dis-

ordered chemisorbed layer is observed, while at higher exposures ($>10^5$ L), the formation of a Cu₂O film sets in. It is generally accepted that within the disordered chemisorbed layer, the positions of the copper atoms are significantly different from those on the clean surface. Although all studies agree on this particular aspect, there is still no clear agreement on the exact structure of the disordered chemisorbed phase.

The earliest structural study by Niehus⁹ was conducted using the low energy ion scattering technique. He discovered a lateral displacement of surface copper atoms and the formation of a “rough” oxygen overlayer with a corrugation of ~ 0.3 Å. Two later studies, using surface-extended x-ray absorption fine structure spectroscopy¹⁰ and surface extended-energy-loss fine-structure spectroscopy,¹¹ attempted to determine the local registry of the chemisorbed species and found the chemisorbed oxygen to occupy a threefold hollow site. This oxygen species was postulated to have partially penetrated the surface layer, causing “rumpling” that results in a lateral expansion of the copper atoms at the hollow site and hence the observation of a roughened surface structure.

Another model based on the mismatch-overlayer structure of the (111) face of Cu₂O and the metal surface was proposed by Jensen *et al.*¹³ This model is rather complex and shares some basic characteristics of the Cu₂O structure. A similar pseudo-Cu₂O overlayer structure was also suggested in Refs. 14 and 15.

In this paper, we present results on the oxidation of Cu(111) and compare them to some published work on 4d transition metals (TM) (Ru, Rh, Pd, Ag).

II. METHODOLOGY AND DEFINITIONS

All calculations are performed using density-functional theory (DFT) and the generalized gradient approximation (GGA) of Perdew, Burke and Ernzerhof¹⁶ for the exchange-correlation functional as implemented in the all-electron

DMol³ code. The DMol³ method employs fast converging three-dimensional numerical integrations to calculate the matrix elements occurring in the Ritz variational method. The wave functions are expanded in terms of a double-numerical quality localized basis set with a real-space cutoff of 9 Bohr. Polarization functions and scalar-relativistic corrections are incorporated explicitly. More details of the DMol³ code can be found elsewhere.^{17,18}

The Cu(111) surface is modeled using a supercell approach, where we use a seven-layered Cu(111) slab with a vacuum region of 25 Å. Oxygen atoms are adsorbed on both sides of the slab, preserving inversion symmetry. We allow full relaxation of the oxygen atoms and all atoms in the outer two Cu substrate layers, while the central three layers of the slab are fixed in their calculated bulk positions. In order to study the effect of oxygen adsorption on the electronic structure and properties of the substrate as a function of coverage Θ , we have considered $\Theta=0.06$ to 1.00 ML. These O adlayer structures are calculated using (4×4) , (3×3) , (2×2) , and (1×1) surface unit cells. We consider adsorption in various on-surface and sub-surface sites. The total energy, force on the atoms, and displacement are converged to within 1×10^{-4} Ha (3×10^{-3} eV), 2.5×10^{-3} Ha/Å (7×10^{-2} eV/Å) and 1×10^{-3} Å, respectively. The Brillouin-zone integrations are performed using a $(12 \times 12 \times 1)$ Monkhorst-Pack (MP) grid for the (1×1) surface unit cell, yielding 19 special \mathbf{k} points in the irreducible surface Brillouin-zone. For the larger surface unit cells, the grids have been folded to obtain the same sampling of reciprocal space. A thermal broadening¹⁹ of 0.1 eV is used to improve the \mathbf{k} -space convergence. To estimate the importance of the various numerical approximations, several test calculations have been performed. For example, we increased the real-space cutoff radius from 9 to 12 Bohr, and found that the change in cohesive energy of Cu was less than 5 meV. A similar difference in the oxygen binding energy was found when a denser $(16 \times 16 \times 1)$ MP grid was used. To determine the error due to the finite slab size, we also tested 9 and 11 atomic layer thick slabs. The difference in binding energy of oxygen $\Delta E_b^{O/Cu}$ was again found to be ± 10 meV. Considering all the test calculations, we estimate the numerical uncertainty for the binding energy differences to be ± 10 meV. As will be shown below, this small uncertainty does not affect our discussion and conclusions.

It is useful to define some quantities which we evaluate in the discussion below. The average binding energy per oxygen atom, for oxygen adsorption on the surface $E_b^{O/Cu}$ is defined as

$$E_b^{O/Cu} = -\frac{1}{N_O} [E^{O/Cu} - (E^{Cu} + N_O E^O)], \quad (1)$$

where N_O is the number of oxygen atoms in the surface unit cell, and the total energies of the adsorbate-substrate system, the clean surface, and the free oxygen atom are represented by $E^{O/Cu}$, E^{Cu} , and E^O , respectively. The binding energy is the energy that a free oxygen atom gains upon adsorption on the Cu surface. It is defined such that a positive number indicates that the adsorption is exothermic (stable) with re-

spect to the free oxygen atom and a negative number indicates that it is endothermic (unstable). The average binding energy can alternatively be referred to the dissociation energy of the O₂ molecule by subtracting half the binding energy of O₂, $E_b^{O_2}$,

$$E_{b(1/2O_2)}^{O/Cu} = E_b^{O/Cu} - \frac{1}{2}(E_b^{O_2}). \quad (2)$$

To analyze the nature of bonding, it is meaningful to consider the difference electron density $n^\Delta(\mathbf{r})$

$$n^\Delta(\mathbf{r}) = n^{O/Cu}(\mathbf{r}) - n^{Cu}(\mathbf{r}) - n^O(\mathbf{r}). \quad (3)$$

Here $n^{O/Cu}(\mathbf{r})$ is the total electron density of the substrate-adsorbate system, from which the electron density of both the clean surface $n^{Cu}(\mathbf{r})$ and that of the isolated oxygen adlayer $n^O(\mathbf{r})$ are subtracted. The atomic positions of the clean Cu surface and O layers are taken to be the ones of the relaxed adsorbate system.

The surface dipole moment (in Debye) is evaluated by the Helmholtz equation

$$\mu = \frac{A\Delta\Phi}{12\pi\Theta}, \quad (4)$$

where A is the area in Å² per (1×1) surface unit cell, and $\Delta\Phi$ is the work-function change in eV. The work function is defined as being the difference between the electrostatic potential in the middle of the vacuum and the Fermi energy of the slab.

To take into consideration realistic experimental conditions, the effect of temperature (T) and pressure (p) is included by explicitly taking into account the surrounding gas phase in terms of “*ab initio* atomistic thermodynamics.”^{2,20,21} This approach allows the determination of the lowest-energy surface structure, for given conditions of a surrounding gas phase, thus enabling the construction of a (p, T) phase diagram containing the stable (or metastable) regions of different phases. This is also an appropriate first approach to steady-state catalysis, which is often run close to thermodynamic equilibrium to prevent catalyst degradation.

We consider a surface in contact with an oxygen atmosphere, which is described by the oxygen pressure and temperature. This atmosphere can then act as a reservoir of oxygen atoms, interchanging oxygen species with the surface, while keeping the temperature and pressure at a constant value. The Gibbs free energy of adsorption can be calculated by

$$\Delta G(T, p) = \frac{1}{A} (G^{O/Cu} - G^{Cu} - \Delta N_{Cu} \mu_{Cu} - N_O \mu_O), \quad (5)$$

where $G^{O/Cu}$ and G^{Cu} are the Gibbs free energies of the O/Cu system and clean surface, respectively. A is the surface area and μ_O and μ_{Cu} are the chemical potentials of the oxygen and copper atoms. The number of oxygen atoms and the difference in the number of Cu atoms between the O/Cu system and clean surface are represented by N_O and ΔN_{Cu} , respectively. When calculating the difference between $G^{O/Cu}$ and G^{Cu} , the contributions due to vibrational free energy,

configurational entropy and the pV term are present. However, from a dimensional analysis, the pV term is of the order of tenths of $\text{meV}/\text{\AA}^2$, hence can be safely neglected.^{20,22} The contribution from configurational entropy is known to be non-negligible at phase transition boundaries,²³ nevertheless it is omitted for this study since we focus on the relative stability of the phases explored rather than the intricate transition boundaries. A more detailed discussion of the vibrational contribution will be presented later in this paper. These aspects simplify Eq. (5) to

$$\Delta G(\Delta\mu_{\text{O}}) \approx \frac{1}{A}(N_{\text{O}}E_{b(1/2\text{O}_2)}^{\text{O/Cu}} - \Delta N_{\text{Cu}}\mu_{\text{Cu}} - N_{\text{O}}\Delta\mu_{\text{O}}), \quad (6)$$

where the oxygen chemical potential is now measured with respect to the dissociation energy of an isolated O_2 molecule $\Delta\mu_{\text{O}} = \mu_{\text{O}} - \frac{1}{2}E_{\text{O}_2}$. As can be easily seen, the term $\Delta N_{\text{Cu}}\mu_{\text{Cu}}$ will only be required when the total number of Cu atoms on the surface is different from that of the clean substrate, and thus represents the cost of interchanging the Cu species with a reservoir of Cu atoms with chemical potential μ_{Cu} . This reservoir is conveniently chosen to be bulk Cu, with which the surface is assumed to be in equilibrium. When comparing a set of surface structures, from Eq. (6), it is clear that the more oxygen accommodated in the structure, the steeper the gradient of the corresponding $\Delta G(\Delta\mu_{\text{O}})$ versus $\Delta\mu_{\text{O}}$ curve will be. In the limiting case of the bulk oxide with an infinite number of O atoms, this will yield a vertical line at a value of oxygen chemical potential that equals the bulk oxide heat of formation per O atom. For values of $\Delta\mu_{\text{O}}$ larger than this (less negative), the bulk oxide represents the thermodynamically stable phase.

At the p and T of interest, oxygen behaves similar to an ideal gas. Then the chemical potential of oxygen μ_{O} can be related to p and T by the formula

$$\mu_{\text{O}} = \frac{1}{2} \left[E_{\text{O}_2} + \tilde{\mu}_{\text{O}_2}(p^0, T) + k_{\text{B}}T \ln \left(\frac{p_{\text{O}_2}}{p^0} \right) \right], \quad (7)$$

where p^0 corresponds to standard pressure and $\tilde{\mu}_{\text{O}_2}(p^0, T)$ includes the contributions from rotations and vibrations of the oxygen molecule, as well as the ideal gas entropy at 1 atmosphere. These are listed in thermodynamic tables and allow the determination of $\tilde{\mu}_{\text{O}_2}$.^{20,24}

III. RESULTS AND DISCUSSION

A. Clean Cu(111), bulk Cu, and the O_2 molecule

Before studying the effect of oxygen adsorption on the Cu(111) surface, we first consider the bulk and clean metal surface systems, and the free oxygen molecule. The calculated lattice constant (neglecting zero point vibrations) is 3.64 \AA , which agrees very well with the established experimental value of 3.61 \AA .²⁵ The computed bulk modulus and cohesive energy are 136 GPa and 3.45 eV , which are in excellent agreement with the experimental values of 137 GPa and 3.49 eV ,²⁵ respectively. The slight overestimation of the lattice constant and the underestimation of the bulk modulus are in line with analogous studies for other TMs.^{26–28}

For the clean surface, we used (1×1) , (2×2) , (3×3) , and (4×4) supercells, including full atomic relaxation of the two outermost Cu layers on each side while keeping the middle three layers fixed at their bulk values. These calculations are required to minimize numerical errors and determine accurately binding energies. The obtained interlayer relaxations $\Delta_{ij} = (d_{ij} - d)/d \times 100\%$, between layers i and j with respect to the bulk spacing $d = 2.10 \text{ \AA}$, are $\Delta_{12} = -0.9\%$ and $\Delta_{23} = -0.3\%$ for the topmost layers. These results are in good agreement with experimental values^{29,30} ($\Delta_{12} = -0.7\%$ and $\Delta_{23} = -0.3\%$), and other DFT calculations.^{31–33} The calculated work function for the clean surface is 4.78 eV and is in line with the reported experimental value³⁴ of 4.94 eV and theoretical value of 4.78 eV .³² The surface energy is determined to be 0.52 eV , which agrees well with reported DFT (0.50 eV) (Ref. 32) and experimental (0.63 eV) (Ref. 35) values.

Spin-unrestricted calculations using non-spherical densities are performed to study the oxygen atom and molecule. To achieve excellent numerical accuracy, the real-space cut-off for the calculation of both the oxygen atom and oxygen molecule is increased to 20 Bohr, with the largest basis set available in the DMol³ code. The binding energy of O_2 is calculated to be 3.04 eV/O atom , while the bond length and vibrational frequency are 1.22 \AA and 1527 cm^{-1} , respectively, in excellent agreement with other theoretical results.^{4,16,26} From experiments, the corresponding values³⁶ are 2.56 eV/atom , 1.21 \AA , and 1580 cm^{-1} . The typical overestimation of DFT-GGA is observed in the binding energy. The calculated values presented here are indicative of well-converged DFT-GGA calculations, and since our interest lies mainly in the relative stability of various structures, this overbinding will not affect the qualitative conclusions in this paper.

B. Oxygen adsorption on Cu(111)

Experimentally, no ordered oxygen adlayers are observed for the Cu(111) surface, unlike for other low-index surfaces.^{37–40} Nevertheless, to build up a systematic study of oxygen interactions on the Cu(111) surface, we have calculated the adsorption energies of O on Cu(111) for a range of coverages Θ (we define Θ as the ratio of the number of adsorbed atoms to the number of atoms in an ideal substrate layer): (1×1) -O ($\Theta = 1.00 \text{ ML}$), (2×2) -3O ($\Theta = 0.75 \text{ ML}$), (2×2) -2O ($\Theta = 0.50 \text{ ML}$), (2×2) -O ($\Theta = 0.25 \text{ ML}$), (3×3) -O ($\Theta = 0.11 \text{ ML}$), and (4×4) -O ($\Theta = 0.06 \text{ ML}$). For on-surface adsorption at each of these coverages, the oxygen adatoms are placed in the fcc- and hcp-hollow, and top sites. We also considered adsorption of oxygen under the first Cu layer. The computed binding energies of both on- and sub-surface adsorption are presented in Fig. 1, with the three sub-surface adsorption sites illustrated.

It is evident that the binding energy of O on Cu(111) changes only marginally, from a coverage of 0.06 to 0.25 ML , but thereafter decreases linearly and sharply, with increasing coverage, indicating a repulsive interaction between surface adsorbates. The fcc-hollow site is energetically slightly more favorable as compared to the hcp-hollow site.

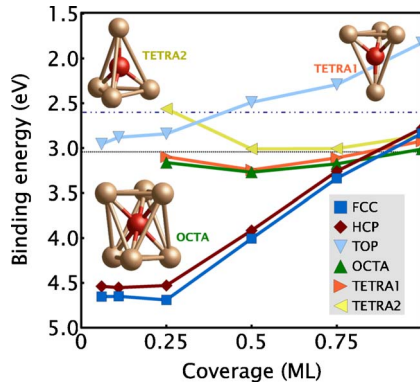


FIG. 1. (Color online) Calculated binding energy of oxygen on Cu(111) in the on-surface and sub-surface sites, for various coverages, with respect to the energy of a free oxygen atom. The solid lines connecting the calculated binding energies are used to guide the eye. Half the binding energy of O_2 , theory and experiment, is indicated by the dotted and dot-dashed horizontal lines, respectively.

The difference of less than 0.15 eV remains constant over the whole considered coverage range. A summary of the various geometric structure parameters for O in the fcc-hollow site at the considered coverages is presented in Table I.

We also calculated the binding energy of oxygen at the bridge site for a coverage of 0.06, 0.25, and 1.00 ML. For 0.06 and 0.25 ML, the binding energies are found to be about 0.40 eV less stable than that in the fcc-hollow sites at the same coverage. This estimated diffusion energy barrier agrees well with the recently reported value⁴ of 0.45 eV obtained for 0.25 ML coverage by a DFT-GGA pseudopotential calculation. However, at 1.00 ML, the difference is narrowed to 0.25 eV. This indicates that the diffusion energy barrier is fairly constant at low coverages and it decreases with increasing coverage, where the dominant interaction is the strong repulsion between O atoms.

When compared to the O/Ag(111) system,²⁶ it clearly shows that the binding energy of oxygen to the Cu(111) surface is much stronger than that of the O/Ag(111) (Ref.

TABLE I. Calculated geometric structure parameters (in Å) for different coverages Θ of O in the fcc-hollow site. d_{Cu-O} indicates the bond length between oxygen and the nearest copper atom and d_{01} is the planar averaged vertical height of O above the topmost Cu layer. d_{12} and d_{23} are the first and second metal interlayer distances where the center of mass of the layer is used. The computed bulk interlayer spacing is 2.10 Å. $E_{p(1/2O_2)}^{O/Cu}$ is the binding energy in eV, with respect to the (calculated) dissociation energy of the oxygen molecule.

Coverage Θ	1.00	0.75	0.50	0.25	0.11	0.06
d_{Cu-O}	1.90	1.89	1.87	1.89	1.90	1.90
d_{01}	1.18	1.14	1.09	1.13	1.14	1.13
d_{12}	2.29	2.14	2.13	2.11	2.10	2.10
d_{23}	2.10	2.10	2.10	2.10	2.11	2.10
$E_{p(1/2O_2)}^{O/Cu}$	-0.21	0.30	0.96	1.65	1.61	1.61

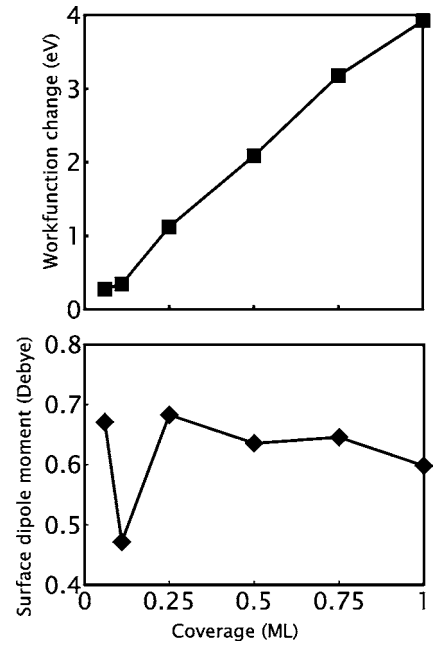


FIG. 2. Calculated work function change $\Delta\Phi$ (top) and surface dipole moment μ (bottom) as a function of coverage for O in the fcc-hollow site. The solid lines connecting the calculated values are used to guide the eye.

26) system. In fact, the binding energy is surprisingly similar to that of the O/Rh(111) (Ref. 28) and O/Pd(111) (Ref. 27) systems. A plausible explanation for the more exothermic binding energy of O on Cu(111) when compared to O/Ag(111), could be derived from the enthalpy of formation of bulk Cu_2O . This is calculated to be -1.24 eV (experimental value⁴¹ -1.75 eV) as compared to the calculated enthalpy of formation²⁶ of Ag_2O of -0.09 eV (experiment -0.33 eV). This indicates that a more rapid oxidation of Cu is to be expected and this is confirmed by various experiments.^{15,42-44} Also, it can be seen that the experimental enthalpy of formation per oxygen atom of Cu_2O is much more similar to that of RuO_2 (-1.59 eV), Rh_2O_3 (-1.19 eV), and PdO (-0.88 eV) than to Ag_2O .^{41,45}

It is seen from Fig. 1 that the binding energies of O at sub-surface sites vary only slightly over the coverages from 0.25 to 1.00 ML, suggesting that the repulsive interaction between the sub-surface oxygens and the energy needed to deform the Cu lattice which typically decreases with increasing coverage compensate each other. Compared to the on-surface binding energies, they are significantly less stable, especially at low coverages. Likewise, this trend is in line with observations for other O/TM systems reported in Ref. 45.

Turning to the electronic properties, we first analyze the change in the calculated work function and surface dipole moment as a function of O coverage, shown in Fig. 2. The work function change increases significantly from 0.11 to 1.00 ML. This can be understood in terms of the large surface dipole moment arising due to partial electron transfer from the surface to the adsorbate; the difference between the electronegativities⁴¹ of oxygen (3.44) and copper (1.90) is quite large ($3.44 - 1.90 = 1.54$). With increasing coverage,

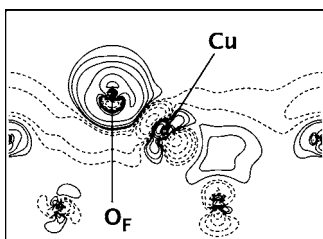


FIG. 3. Difference electron density plot in the $[\bar{2}11]$ plane perpendicular to the Cu(111) surface with a 0.25 ML coverage of oxygen at the fcc-hollow site. The dashed lines represent charge depletion and the solid lines represent charge accumulation. The lowest positive contour line is at 0.001 electron Bohr $^{-3}$, while the highest negative contour line corresponds to a value of -0.001 electron Bohr $^{-3}$. In between, the electron density changes successively by a factor of $10^{1/3}$ electron Bohr $^{-3}$.

there will be a strong repulsion amongst the partially negatively charged O atoms. To reduce this repulsion, there will be partial electron transfer back to the substrate, giving rise to a decrease in the surface dipole moment, resulting in a depolarization. The sharp dip in the surface dipole moment at 0.11 ML can be correlated to a smaller electron charge (per \AA^3) on the O atom as compared to the lower and higher coverage structures. The abovementioned increase in the work function with increasing oxygen coverage is similar to the late $4d$ TM-oxygen systems.^{27,28} Comparing the work-function change at 0.25 ML O coverage of the O/Cu (1.17 eV), a $3d$ TM-oxygen system and its late $4d$ TM [Ru (0.40 eV), Rh (0.55 eV), and Pd (0.48 eV)] counterparts, we find that the work function changes of the latter are considerably smaller than for O/Cu. This can be understood by considering the electronegativities of Pd (2.20), Rh (2.28), and Ru (2.20). The resulting smaller differences between the electronegativities of oxygen and these TMs give rise to the smaller observed work function changes. Since Cu is slightly more electropositive than the abovementioned $4d$ metals, a large work function change is to be expected for the O/Cu system. Silver, having a similar electronegativity (1.93) to that of Cu, experiences a similar work function change (1.25 eV) upon O adsorption to the O/Cu system at the same coverage.

The adsorbate dipole moment is a direct consequence of the adsorbate induced redistribution of the electron density. To gain further insight into the electronic structure of O/Cu(111), the difference electron density plot, $n^A(\mathbf{r})$, for 0.25 ML coverage presented in Fig. 3 is considered next. The corresponding projected density-of-states (PDOS) is shown in Fig. 4. We have chosen to use plots for the 0.25 ML coverage to understand the electronic effects for two reasons: It can be seen in Fig. 2 that the surface dipole moment saturates at coverages higher than 0.25 ML. On the other hand, binding energies for O coverages less than 0.25 ML are very similar. Hence we have chosen the 0.25 ML coverage as a point of reference for the following discussion.

The difference electron density $n^A(\mathbf{r})$ is shown for a plane perpendicular to the surface, containing the Cu-O bond. This quantity is more instructive than a total density plot as it

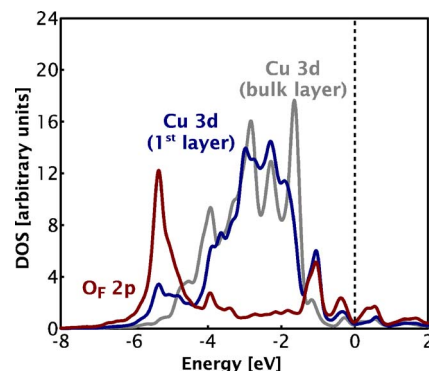


FIG. 4. (Color online) Projected density-of-states for the O/Cu(111) system with O in the fcc-hollow site at coverage 0.25 ML. The Fermi energy is indicated by the vertical dotted line at 0 eV.

clearly focuses only on the change in electron density due to O adsorption, making it sensitive to small amounts of electron transfer. As expected, the perturbation created by the oxygen adsorption is mostly localized on the O atom itself and on its nearest Cu neighbor. The electron density of the nearest-neighbor Cu is depleted (shown as dotted lines) with a corresponding enhancement in the electron density of the O adatom (shown as solid lines). The electron transfer from the Cu atom to the O adatom is significant and reflects the high electronegativity of oxygen. This results in an accumulation of electron density at the vacuum side of the surface, with an induced inward pointing dipole moment. Considering the observations made concerning Figs. 2 and 3, it is evident that the high electronegativity of oxygen is responsible for both the large work function change and significant polarization, indicating some degree of ionic character in the Cu-O bond formed.

By looking at the corresponding PDOS, it can be seen that there is a renormalization (i.e., a broadening and shifting) of the O atomic energy levels to lower energies and a hybridization between the O $2p$ and Cu $3d$ orbitals. The oxygen levels are split into bonding and antibonding states.⁴⁶ The bonding state is located at the bottom, and outside, of the Cu $3d$ band and is fully occupied, while the antibonding states are found at the top of the Cu $3d$ band and are only partially occupied and have a minimum in the PDOS at the Fermi level. The weight being on the side of the bonding states results in a much stronger bond between oxygen and the Cu surface as compared to O/Ag,²⁶ where the antibonding states are more pronounced, thereby weakening the bonding between Ag and O.

C. Bulk cuprous oxide, Cu $_2$ O

Before studying possible surface oxidic structures, it is useful to consider the properties and structure of bulk copper oxide. The two most common oxides of Cu are cuprous oxide Cu $_2$ O and cupric oxide CuO. The former has a cuprite structure and the latter crystallizes in a tenorite structure. The cuprite structure of Cu $_2$ O is shown in Fig. 5(A). The standard enthalpies of formation⁴¹ for Cu $_2$ O and CuO are -1.75 and -1.64 eV, showing that from a thermodynamic point of

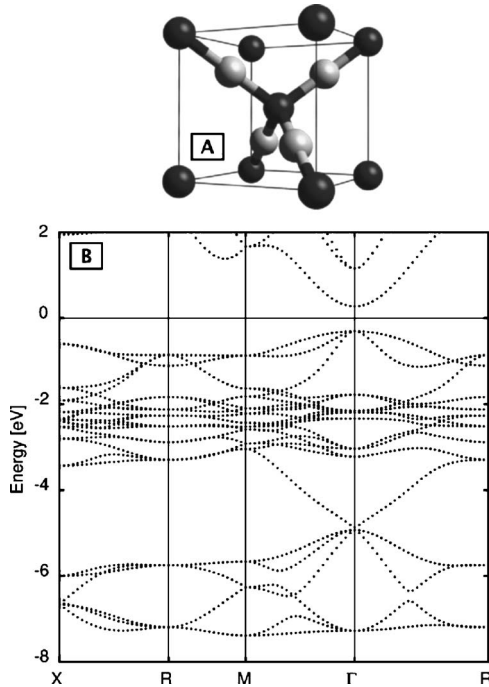


FIG. 5. (A) The crystal structure of cuprous oxide Cu_2O . The oxygen and copper atoms are represented by black and pale gray circles, respectively. (B) The band structure of Cu_2O . The calculated band gap for Cu_2O is 0.64 eV.

view, Cu_2O forms more readily than CuO . We have chosen to focus on cuprous oxide for our investigation as recent studies^{42,43,47} have shown that the Cu_2O phase is most commonly seen upon oxidation of Cu. The reduction of CuO by Cu to Cu_2O is exothermic⁴⁸ at room temperature and is even more so at elevated temperatures, while its reduction to Cu by thermal desorption of oxygen is highly endothermic, even at high temperatures. Hence it is valid to assume in our study the formation of a cuprous oxide phase.

The calculation for cuprous oxide is performed using a six atom cell (Cu_4O_2), and describing the irreducible Brillouin-zone with 56 special \mathbf{k} points. The real-space cutoff of 9 Bohr is also used in this calculation. We have determined the lattice constant, bulk modulus and enthalpy of formation for cuprous oxide and they are 4.32 Å, 103.7 GPa, and 1.24 eV, respectively. The former two quantities agree quite well with both experimental and theoretical values, summarized in Table II. The theoretical enthalpy of formation $H_{\text{Cu}_2\text{O}}^f$ is considerably smaller than the experimental value and this can in part be attributed to the notable typical overestimation of the binding energy of the oxygen molecule. Calculated bond distances are slightly larger (not more than 2%) than the experimental values which is not unusual for DFT-GGA calculations.

The band structure of cuprous oxide is shown in Fig. 5(B). At the Γ point, it can be clearly seen that Cu_2O is a direct band gap semiconductor, with a theoretical band gap of 0.64 eV. The well-established experimental value²⁵ is 2.17 eV and typically, significantly larger than that obtained by DFT-GGA (or LDA).

TABLE II. Bulk properties of cuprous oxide, Cu_2O . The lattice constant a_0 , the nearest distance between copper atoms $d_{\text{Cu-Cu}}$ and oxygen atoms $d_{\text{O-O}}$, and the Cu-O bond length $d_{\text{Cu-O}}$ are listed in units of Å. The bulk modulus B_0 and enthalpy of formation $H_{\text{Cu}_2\text{O}}^f$ are given in GPa and eV per oxygen atom, while the band gap E_{bg}^f is in eV.

	a_0	$d_{\text{Cu-Cu}}$	$d_{\text{O-O}}$	$d_{\text{Cu-O}}$	B_0	$H_{\text{Cu}_2\text{O}}^f$	E_{bg}^f
Present work	4.32	3.05	3.74	1.87	104	1.24	0.64
PWPP ^a	4.34	3.07		1.88	104		
FPLAPW ^b	4.30	3.04		1.86	108		0.50
HF ^c	4.28	3.03		1.85	93		9.70
Experiment ^d	4.27	3.02	3.68	1.84	112	1.75	2.17

^aReference 49.

^bReference 50.

^cReference 51.

^dReferences 41 and 52–54.

D. Surface oxidic structures

Further oxidation of the Cu surface might lead to the formation of surface and/or bulk oxides as observed on other late TM surfaces. Many experiments^{42–44,47,55} have reported the formation of $\text{Cu}_2\text{O}(111)$ on the $\text{Cu}(111)$ surface upon oxidation. Keeping this in mind, we consider various oxidic structures and determined their relative stability.

Recent UHV scanning tunneling microscopy experiments¹⁵ have shown that oxidation of the $\text{Cu}(111)$ surface is extremely complex. Observed surface structures are described as a $(\sqrt{73}R5.8^\circ \times \sqrt{21}R10.9^\circ)$ structure (also known as the “44” structure) and a $(\sqrt{13}R46.1^\circ \times 7R21.8^\circ)$ structure (also known as the “29” structure). These phases are reported to resemble the basic structure of one layer of $\text{Cu}_2\text{O}(111)$ which consists of a three-layer repeat unit with each copper layer sandwiched between two layers of oxygen atoms. The surface unit cell possesses a hexagonal symmetry and has approximately twice the surface unit area of $\text{Cu}(111)$. To mimic these complex surface structures, we have used a (2×2) and a (4×4) supercell to model various possible structures, with only the most energetically favorable phases shown in Fig. 6.

We have classified the investigated structures into two “families:” The $p2$ -configuration and the $p4$ -configuration. The former relates to the use of a (2×2) periodicity and the latter to a (4×4) periodicity, with respect to the clean surface. All proposed oxidic structures consist of a basic three-layer lateral unit with a copper layer sandwiched between two layers of oxygen atoms: an upper layer of oxygen on top of the Cu layer O_U and a lower layer O_L . We consider this O-Cu-O lateral unit as a trilayer (TL) which is characteristic of the (111) surface of bulk Cu_2O .⁴⁹

To expand and include the possibility of other oxidic structures with varying oxygen content, oxygen and copper adatoms are further adsorbed onto or removed from the surface. These adatoms are denoted by X_F , X_H , and X_T (where $X=\text{O}$ or Cu), indicating the adsorption site to be a fcc-, a hcp-hollow, or a top site of the Cu substrate, respectively. To illustrate this point with an example, we consider the $p4$

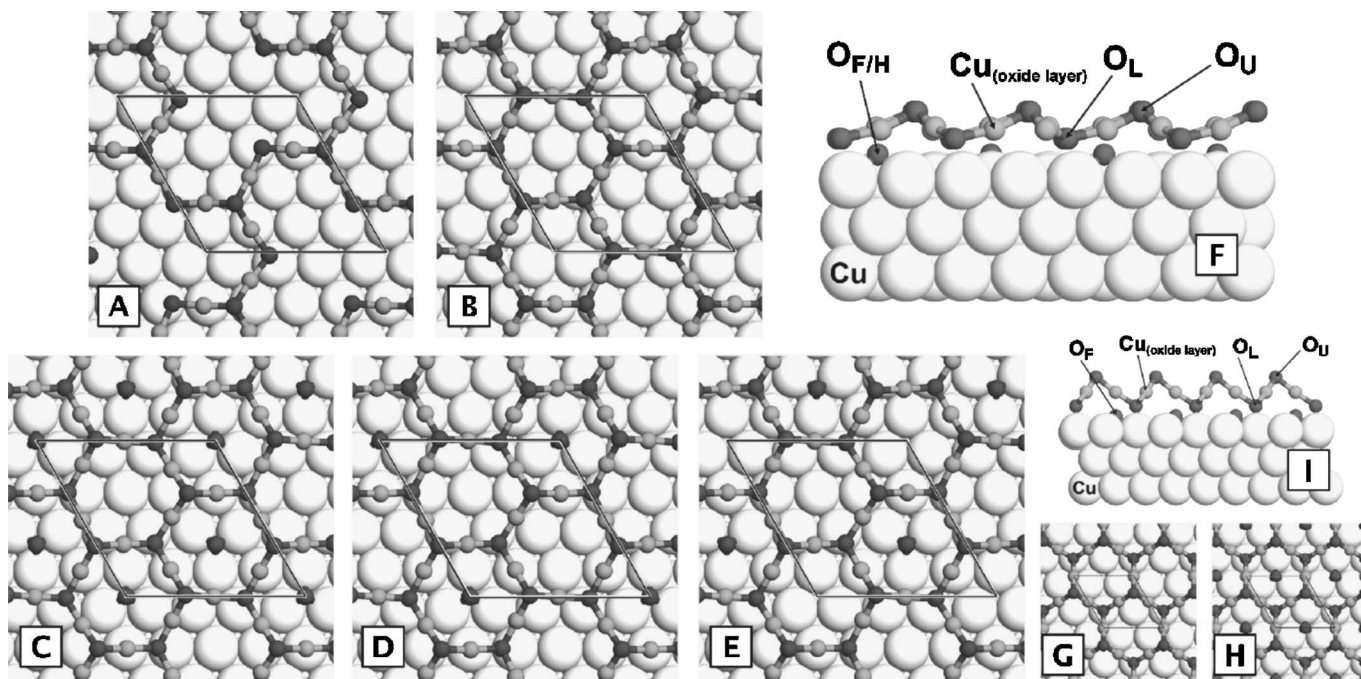


FIG. 6. Optimized $p4$ - and $p2$ -configuration oxidic structures. (A) $p4$ - OCu_3 , (B) $p4$, (C) $p4+\text{O}_{FH}$, (D) $p4+\text{O}_F$, (E) $p4+\text{O}_H$, and (F) the side view of the $p4$ -configuration structures. (G) and (H) are the unstable $p2$ and $p2+\text{O}_F$ structures. The side view of the $p2$ -configuration is shown in (I). The surface unit cell is indicated by the solid lines. The unreconstructed Cu layer is shown as large white circles, with the oxide layer Cu atoms in small light gray circles. Oxygen atoms are denoted by small dark gray circles.

$+\text{Cu}_T+\text{O}_F$ structure; it would comprise the basic $p4$ structure with an additional (hence the “+” sign) Cu adatom at the top site and O at the fcc-hollow site. Furthermore, the notation $p4+\text{O}_{FH}$ would mean the addition of O adatoms at both the fcc- and hcp-hollow sites simultaneously.

The removal of a so-called “ OCu_3 ” unit from the $p4$ structure results in the “ $p4$ - OCu_3 ” structure [Fig. 6(A)]. The “ OCu_3 ” unit can be understood as an oxygen atom bonded to three Cu atoms in a pyramidal geometry. The average binding energy of the $p4$ - OCu_3 structure is very similar to that of the most favorable on-surface structure ($\Theta=0.25$ ML) described in the previous section, with a difference of only 1 meV between them. By removing another “ OCu_3 ” unit, this would produce the structure $p4$ -(OCu_3)₂, and this can be understood as a pyramidal structure formed by 4 oxygen atoms at the vertices of a 3 Cu atom cluster. This structure could be seen as the initial stage of surface oxide formation, and by adding two “ OCu_3 ” units, the $p4$ structure would result. Similarly to the homogeneous oxygen overlayer discussed in the previous section, the oxidic layer is formed on both sides of the slab to preserve inversion symmetry and uses the converged parameters determined for the (2×2) and (4×4) supercells. The average binding energy of oxygen for each of the considered oxidic structures is presented in Table III.

Upon close examination of Figs. 6(F) and 6(I), one can observe that the Cu-O-Cu angle (relative to the surface normal) of the $p2$ -configuration structures is smaller than that of the $p4$ -configuration structures. Given that the Cu-O bond length in both configurations are rather similar ($p4$ -configuration: 1.83 Å and $p2$ -configuration: 1.82 Å), one can estimate the degree of buckling by measuring the

Cu-O-Cu angle in the TL. For bulk Cu_2O , the Cu-O-Cu angle is 109.0°. For the $p2$ - and $p4$ -configuration structures, this angle is found to be smaller. It is averaged at 101.3° and 86.7° for the $p4$ - and $p2$ -configuration, respectively. The 20% decrease in the Cu-O-Cu angle of the $p2$ -configuration as compared to that in $\text{Cu}_2\text{O}(111)$ indicates that the $p2$ -configuration structures suffer, amongst other unfavorable interactions, from a stronger lateral repulsion between the O at

TABLE III. Binding energies, cf. Eq. (2) (with respect to the calculated $\frac{1}{2}\text{O}_2$) of oxidic structures at corresponding oxygen coverages.

Oxidic structures	Coverage (ML)	E_b (eV)	Figure
$p2$	0.500	1.14	6(G)
$p2+\text{Cu}_F$	0.500	1.17	
$p2+\text{O}_F$	0.750	1.26	6(H)
$p4$	0.375	1.64	6(B)
$p4+\text{Cu}_T$	0.375	1.48	
$p4+\text{Cu}_H$	0.375	1.59	
$p4+\text{Cu}_{FH}$	0.375	1.53	
$p4+\text{Cu}_{HT}$	0.375	1.42	
$p4+\text{Cu}_T+\text{O}_F$	0.438	1.48	
$p4+\text{O}_F$	0.438	1.60	6(D)
$p4+\text{O}_H$	0.438	1.58	6(E)
$p4+\text{O}_{FH}$	0.500	1.54	6(C)
$p4-\text{OCu}_3$	0.313	1.65	6(A)
$p4-(\text{OCu}_3)_2$	0.250	1.58	

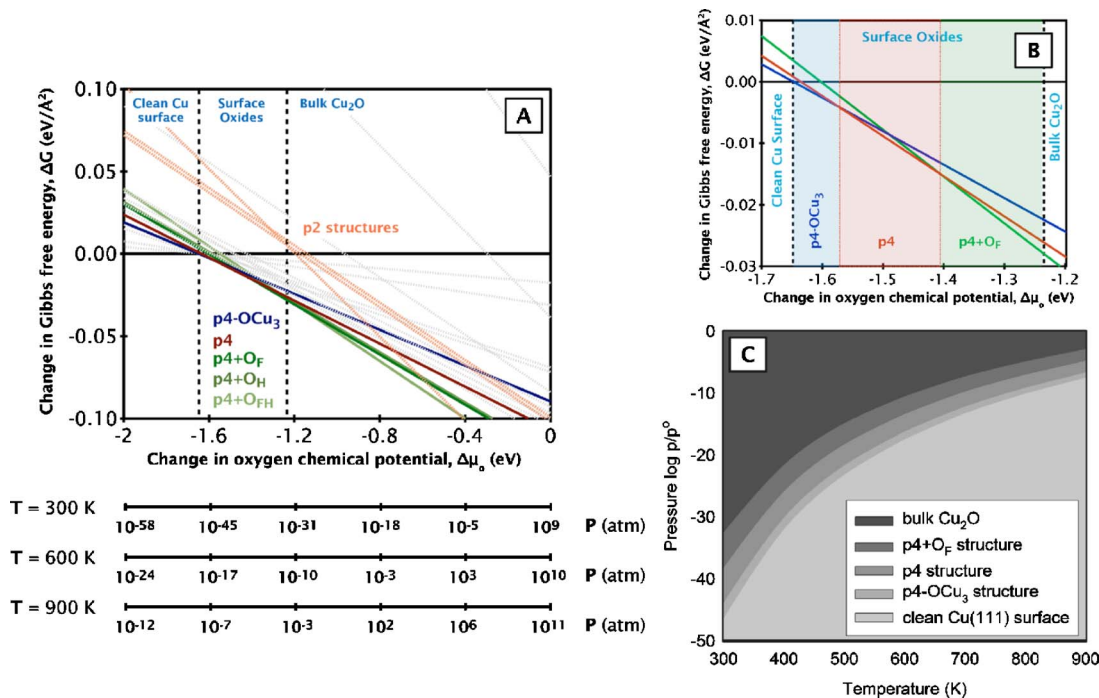


FIG. 7. (Color online) (A) Calculated Gibbs free energy of adsorption ΔG for a clean Cu(111) surface and other oxygen-containing surface structures, with varying oxygen chemical potential $\Delta\mu_{\text{O}}$. All unfavorable surface phases are indicated by light gray dotted lines, with the $p2$ -configuration phases in orange. The phases of $p4\text{-OCu}_3$ and $p4$ are represented by the dark blue and red lines, respectively. The $p4\text{+O}_F$, $p4\text{+O}_H$, and $p4\text{+O}_{FH}$ phases show similar stability and are presented in varying shades of green lines. (B) shows the same as (A) but on a larger scale. (C) The stability range of the mentioned phases, evaluated in (A), plotted in the (p, T) space. The phases are distinguished by varying shades of gray, with the bulk oxide phase more favorable at high pressure for all temperatures considered.

oms in the TL. The strain is less severe in the $p4$ -configuration structures, where the difference in the Cu-O-Cu angle is only 7%. The thickness of the TL in the $p4$ -configuration structures is determined to be 1.20 \AA and that of the $p2$ -configuration structures to be 2.12 \AA . Compared to the thickness of 1.22 \AA found in $\text{Cu}_2\text{O}(111)$, the TL in the $p4$ -configuration structures is only 1.6% smaller in the z direction whereas that of the $p2$ -configuration structures is 76.3% greater. Together with the much smaller Cu-O-Cu angle, this results in a huge compressive stress in the oxide-like surface structure and hence destabilizes the $p2$ -configuration structures greatly. To critically assess the strain experienced by the $p4$ -configuration structures, we can see that the surface unit area of $\text{Cu}_2\text{O}(111)$ is different to what it would be “forced” to have in the (4×4) surface unit cell, namely: using the calculated bulk oxide lattice constant gives a surface unit area of 32.27 \AA^2 . If the TL of this oxide is forced to be in the (4×4) cell of the Cu(111) surface, the corresponding area is 30.84 \AA^2 , i.e., it would be compressed by 4.4%. Or equivalently, assuming the bulk angle of 109° , it would mean that the Cu-O bond length $d_{\text{Cu-O}}$ of these oxidic structures would be compressed by $(1.87 - 1.83)/1.87 \times 100\% = 2.1\%$, compared to that in the ideal oxide surface structure. If this strain could be reduced by forming surface oxides over larger regions of Cu(111) (such as the “44” and “29” structures), the relief of strain may result in a more favorable energy. Given the small differences in the structural parameters of the bulk Cu_2O and the $p4$ -configuration structures, we find it a reasonable model to represent the

O/Cu(111) system, even though it has a smaller periodicity than the “44” and “29” structures, as seen in experiments.

E. Thermodynamic phase diagram of the O/Cu(111) system

We investigate the effect of pressure and temperature on the stability of the various oxidic structures. To incorporate these effects, we calculate the Gibbs free energy of the phase of interest as a function of oxygen chemical potential [see Eqs. (5) and (6)]. The result is presented in Figs. 7(A) and 7(B) (on a larger scale). The variation of the energy with the chemical potential of oxygen is reflected in the gradient of the lines. The steeper the gradient, the higher the O coverage. We have also inserted the corresponding pressure-temperature bar lines for $T = 300, 600,$ and 900 K . These reflect a span of pressure values used in industrially relevant conditions.

Using Eq. (7), the above results can be presented as the two-dimensional phase diagram shown in Fig. 7(C). From previous studies,^{20,21} the estimated error bar for the pressure and temperature scale is approximately 10^3 atm and $\pm 100\text{ K}$, respectively. Hence caution has to be taken not to indulge in attributing too much meaning to the absolute values presented, but rather to use them in a qualitative discussion to help distinguish the relative stability of the various phases of interest. In addition to the pressure and temperature error bars, the vibrational contribution to the differences in Gibbs

free energy has to be checked, especially at high temperatures where this contribution may be significant. This contribution can be obtained from the phonon density-of-states, computed from DFT. However, for simplicity, by applying the Einstein approximation²⁵ to the phonon DOS, one can estimate the order of the magnitude of this contribution. We adopt the approach used in Ref. 20 and calculated the characteristic vibrational modes of Cu (20 meV) and O (62 meV) in bulk Cu₂O. This is done by performing a frequency calculation for each atom type in Cu₂O and averaging the vibrational modes due to each Cu and O. These averaged values are comparable to the reported values for PdO (Ref. 22) and RuO₂ (Ref. 20) and even a $\pm 50\%$ variation of the values yields a change of less than 10 meV/Å². Thus, for the present system, vibrations may be neglected, not affecting the physical conclusions drawn. Such a course of action is however not always justified. Recent studies⁵⁶ have found that hydroxylated surfaces have a large vibrational contribution to the surface free energy which is of the order of 15 to 30 meV/Å². They need to be included to draw meaningful conclusions, which calls for additional care when the technique of first-principles atomistic thermodynamics is employed. When using this technique, one also has to take caution to try and include all conceivable relevant structures, that is, to sample as complete a configurational space as possible. Structures that are not considered will not appear in the phase diagram.

It can be seen that for values of the oxygen chemical potential of less than -1.65 eV, the clean Cu(111) surface is the thermodynamically most stable phase. For higher values of oxygen chemical potential from -1.65 to -1.24 eV, the $p4$ -OCu₃, $p4$ and $p4+O_F$ structures are the most thermodynamically favored [see Figs. 7(A) and 7(B)]. Within the accuracy of our calculations, they are proposed to be almost degenerate, showing minimal variation, before the onset of the bulk oxide phase at an oxygen chemical potential of -1.24 eV. It is also interesting to point out that we have found none of the on-surface chemisorbed overlayers to be stable for any value of the oxygen chemical potential, demonstrating that the oxidation of Cu does not proceed via such ordered structures which are often seen on other TM surfaces.

After identifying the lowest energy configuration of those considered, it is interesting to look at their electronic properties. We have plotted both the difference electron density distribution $n^{\Delta}(\mathbf{r})$ along the O-Cu-O bond direction, and the PDOS of the three oxidic structures and the bulk oxide and presented them in Figs. 8 and 9, respectively. Our aim is to identify any correlation between the electronic structure of the surface oxidic structures and the bulk oxide, in addition to the structural similarity seen in the previous section. We can see from both the $n^{\Delta}(\mathbf{r})$ and the PDOS that these surface oxidic structures exhibit features quite similar to the bulk oxide phase. Similarly to the homogeneous adsorption of O on Cu(111), the oxygen atoms, O_U and O_L interact strongly with the central Cu layer atom, depleting the electron density of Cu and inducing a significant enhancement of the electron

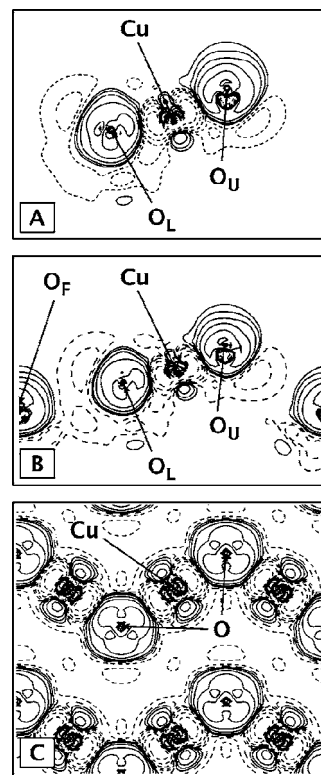


FIG. 8. Difference electron density plot of oxidic structures and the bulk oxide phase: (A) $p4$, (B) $p4+O_F$, and (C) bulk Cu₂O. The dashed lines represent charge depletion and the solid lines represent charge accumulation. The contour line values are the same as stated in Fig. 3.

density at the O atoms. The redistribution of electron density occurs mainly in the TL and this is clearly seen along the O-Cu-O bond. Upon close inspection of Figs. 8(A) and 8(B), one will realize that the difference electron density distribution of O_L is subtly different from O_U and O_F . This can be attributed to the chemical environment of these various O adatoms. O_L has a higher coordination of Cu atoms [see Fig. 6(D)] as compared to the other two O adatoms, and this is reflected in a more evenly distributed difference electron density around O_L . This is also true for the O atoms in the bulk oxide [Fig. 8(C)] where they occupy higher coordination sites as opposed to surface oxygen adatoms. From the PDOS plots, three distinct features can be gathered. Moving from the $p4$ -OCu₃ structure to the $p4+O_F$ structure and the bulk Cu₂O phase sequentially, a shift in the hybridized O-2p-Cu-3d band to lower energy (i.e., to the left of the Fermi level) and a narrowing of the Cu 3d band can be seen. Figure 9(C) shows that the additional O adatom in the fcc-hollow site in the $p4+O_F$ is responsible for the formation of the peak seen at about -1 eV in Fig. 9(D). The peaks around -5.8 and -7.5 eV can be related to the O 2p states of the O_L atom and resemble the features of the bulk oxide, once more highlighting the resemblance between the bulk oxide and the surface oxidic structures. These features suggest to us that these oxidic structures could well be precursor states that could be stabilized under UHV conditions. From our study,

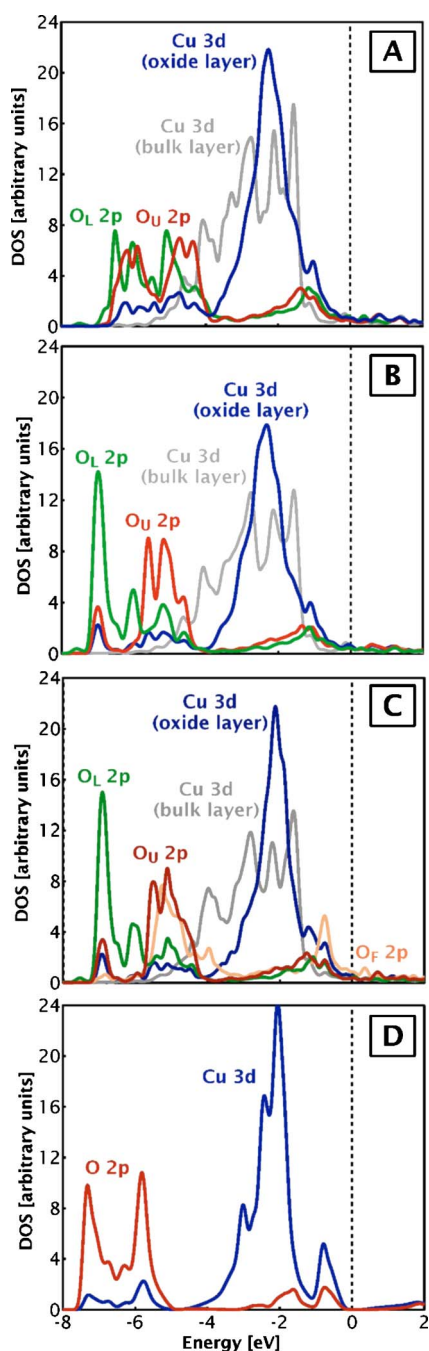


FIG. 9. (Color online) Projected density-of-states for the favored oxidic structures and bulk oxide phase: (A) $p4\text{-OCu}_3$, (B) $p4$, (C) $p4+O_F$, and (D) bulk Cu_2O . The Fermi energy is indicated by the vertical dotted line at 0 eV.

we cannot determine the lifetime of these precursor states as kinetics is not explicitly included, however, it does give us a clue as to how the bulk oxide might be formed via these precursor states.

Having discussed both the geometric and electronic structure of the O/Cu(111) system, we can now turn our attention to its relevance to copper-based catalysis under working conditions. From the constructed (p, T) phase diagram [Fig. 7(C)] one can make an educated first guess towards the relevance of a given phase for catalysis. For copper-based cata-

lysts in the low-temperature water-gas shift reaction, the typical operational conditions are 1 atm and 600 K. Deactivation of this catalyst occurs at higher temperatures due to sintering.⁵⁷ Hence from the (p, T) phase diagram, the bulk oxide is identified to be the thermodynamically most stable phase, given the assumption that kinetic effects are negligible.

Comparing to other reported (p, T) phase diagrams for O/Ag(111),² O/Pd(111),⁵⁸ O/Rh(111),^{59,60} and O/Ru(0001),² we find that though the O/Cu(111) system shows a qualitatively similar trend to them, they exhibit marked differences in behavior. For the O/Ag(111) and O/Pd(111) systems, oxidation of the metal surface results in the formation of an on-surface chemisorbed adlayer of oxygen. Upon further oxidation, a thin surface oxide is formed and eventually followed by the bulk oxide phase. For both the O/Ru(0001) and O/Rh(111) systems, this transition from the metal surface to the bulk oxide phase is facilitated only by on-surface oxygen adlayers, i.e., without the formation of surface oxides. However, for the O/Cu(111) system, we find that upon increasing the oxygen chemical potential, the bulk oxide phase forms rapidly via surface oxidic structures, without the formation of any favorable on-surface oxygen adlayer. Hence it can be seen that oxidation of TMs is a rather complex process and more detailed investigations are required. For this study, we can only suggest on thermodynamic grounds that the bulk oxide phase is the stable phase under industrial catalytic conditions. With regard to the experimentally observed reconstructed oxidic structures, matching the pressure (10^{-13} atm) and temperatures (473 to 773 K) mentioned in Ref. 15, the complicated 29- and 44-oxide structures seem to coincide with the oxidic structures we predicted, within the error limits mentioned above.

Recently, a new oxygen-induced $p(4 \times 4)$ reconstruction of the Ag(111) surface has been identified which shows considerably better agreement with experimental results than all previously proposed models.^{61,62} We have modeled this similar oxidic structure for the O/Cu(111) system (with coverage ≈ 0.375 ML) and found an identical surface relaxation as to that mentioned in Refs. 61 and 62. However, its oxygen binding energy (1.50 eV) is less favorable than those of the identified surface oxides shown in Fig. 6 (see Table III).

IV. SUMMARY AND CONCLUSION

In this paper, we presented a systematic DFT-GGA study of the chemisorption of oxygen and the formation of oxidic structures on the Cu(111) surface. We provided results for energetics and structural and electronic properties of the system. By comparing with reported studies for O/Ru(0001), O/Rh(111), O/Pd(111), and O/Ag(111), we are able to both identify and differentiate trends found for these $4d$ transition metal surfaces. By incorporating pressure and temperature effects, we find that oxygen does not form chemisorbed adlayers on the Cu(111) surface but proceeds directly to the formation of surface oxidic structures and the bulk oxide

phase, which is in contrast to the $4d$ metals but in line with experimental observation. At catalytic working conditions, the bulk oxide phase is clearly found to be the most thermodynamically stable phase and hence it should be considered as an active catalytic phase in technologically relevant reactions.

ACKNOWLEDGMENTS

The authors gratefully acknowledge support from the Australian Research Council (ARC), the Australian National Supercomputing Facility (APAC), and the Australian Centre for Advanced Computing and Communications (ac3).

*Corresponding author. Electronic mail: aloysius@physics.usyd.edu.au

- ¹C. Stampfl, M. V. Ganduglia-Pirovano, K. Reuter, and M. Scheffler, *Surf. Sci.* **500**, 368 (2002).
- ²C. Stampfl, *Catal. Today* **105**, 17 (2005).
- ³A. Y. Rozovskii and G. I. Lin, *Top. Catal.* **22**, 137 (2003).
- ⁴Y. Xu and M. Mavrikakis, *Surf. Sci.* **494**, 131 (2001).
- ⁵G. Ertl, *Surf. Sci.* **6**, 208 (1967).
- ⁶A. Spitzer and H. Luth, *Surf. Sci.* **118**, 136 (1982).
- ⁷R. W. Judd, P. Hollins, and J. Pritchard, *Surf. Sci.* **171**, 643 (1986).
- ⁸M. K. Rajumon and C. N. R. R. K. Prabhakaran, *Surf. Sci.* **233**, L237 (1990).
- ⁹H. Niehus, *Surf. Sci.* **130**, 41 (1983).
- ¹⁰J. Haase and H. J. Kuhr, *Surf. Sci.* **203**, L695 (1988).
- ¹¹B. Luo and J. Urban, *J. Phys.: Condens. Matter* **3**, 2873 (1991).
- ¹²R. L. Toomes, D. P. Woodruff, M. Polcik, S. Bao, P. Hofmann, and K. M. Schindler, *Surf. Sci.* **443**, 300 (2000).
- ¹³F. Jensen, F. Besenbacher, E. Lægsgaard, and I. Stensgaard, *Surf. Sci.* **259**, L774 (1991).
- ¹⁴S. M. Johnston, A. Mulligan, V. Dhanak, and M. Kadodwala, *Surf. Sci.* **519**, 57 (2002).
- ¹⁵T. Matsumoto, R. Bennett, P. Stone, T. Yamada, K. Domen, and M. Bowker, *Surf. Sci.* **471**, 225 (2001).
- ¹⁶J. P. Perdew, K. Burke, and M. Ernzerhof, *Phys. Rev. Lett.* **77**, 3865 (1996).
- ¹⁷B. Delley, *J. Chem. Phys.* **92**, 508 (1990).
- ¹⁸B. Delley, *J. Chem. Phys.* **113**, 7756 (2000).
- ¹⁹M. Weinert and J. W. Davenport, *Phys. Rev. B* **45**, 13709 (1992).
- ²⁰K. Reuter and M. Scheffler, *Phys. Rev. B* **65**, 035406 (2002).
- ²¹W. X. Li, C. Stampfl, and M. Scheffler, *Phys. Rev. B* **68**, 165412 (2003).
- ²²J. Rogal, K. Reuter, and M. Scheffler, *Phys. Rev. B* **69**, 075421 (2004).
- ²³K. Reuter and M. Scheffler, *Phys. Rev. Lett.* **90**, 046103 (2003).
- ²⁴D. R. Stull and H. Prophet, *JANAF Thermochemical Tables* (U.S. National Bureau of Standards, Washington, DC, 1971), 2nd ed.
- ²⁵C. Kittel, *Introduction to Solid State Physics* (Wiley, New York, 1996).
- ²⁶W. X. Li, C. Stampfl, and M. Scheffler, *Phys. Rev. B* **65**, 075407 (2002).
- ²⁷M. Todorova, K. Reuter, and M. Scheffler, *J. Phys. Chem. B* **108**, 14477 (2004).
- ²⁸M. V. Ganduglia-Pirovano and M. Scheffler, *Phys. Rev. B* **59**, 15 533 (1999).
- ²⁹S. A. Lindgren, L. Walldén, J. Rundgren, and P. Westrin, *Phys. Rev. B* **29**, 576 (1984).
- ³⁰S. P. Tear, K. Röhl, and M. Prutton, *J. Phys. C* **14**, 3297 (1981).
- ³¹A. Groß, *Theoretical Surface Science: A Microscopic Perspective*

- (*Advanced Texts in Physics*) (Springer, Berlin, 2002).
- ³²J. F. Da Silva, C. Stampfl, and M. Scheffler, *Surf. Sci.* **600**, 703 (2006).
- ³³T. Rodach, K. Bohnen, and K. Ho, *Surf. Sci.* **286**, 66 (1993).
- ³⁴J. Hölzl, F. Schulte, and H. Wagner, *Work Functions of Metals, in Solid Surface Physics* (Springer, Berlin, Heidelberg, 1979), Vol. 85.
- ³⁵W. R. Tyson and W. A. Miller, *Surf. Sci.* **62**, 267 (1977).
- ³⁶K. Huber and G. Herzberg, *Molecular Spectra and Molecular Structure IV: Constants of Diatomic Molecules* (Van Nostrand Reinhold, New York, 1979).
- ³⁷I. Merrick, J. E. Inglesfield, and H. Ishida, *Surf. Sci.* **551**, 158 (2004).
- ³⁸M. Wuttig, R. Franchy, and H. Ibach, *Surf. Sci.* **224**, L979 (1989).
- ³⁹T. Lederer, D. Arvanitis, G. Comelli, L. Tröger, and K. Baberschke, *Phys. Rev. B* **48**, 15390 (1993).
- ⁴⁰F. Besenbacher and J. K. Nørskov, *Prog. Surf. Sci.* **44**, 5 (1993).
- ⁴¹D. R. Lide, *CRC Handbook of Chemistry and Physics, Internet version 2005* (CRC Press, Boca Raton, FL, 2005).
- ⁴²L. Zhou, S. Günther, D. Moszynski, and R. Imbihl, *J. Catal.* **235**, 359 (2005).
- ⁴³J. F. Pierson, D. Wiederkehr, and A. Billard, *Thin Solid Films* **478**, 196 (2005).
- ⁴⁴L. H. Dubois, *Surf. Sci.* **119**, 399 (1982).
- ⁴⁵M. Todorova, W. X. Li, M. V. Ganduglia-Pirovano, C. Stampfl, K. Reuter, and M. Scheffler, *Phys. Rev. Lett.* **89**, 096103 (2002).
- ⁴⁶M. Scheffler and C. Stampfl, *Handbook of Surface Science* (Elsevier Science, Amsterdam, 2000), Vol. 2, chap. Theory of Adsorption on Metal Surface, p. 285.
- ⁴⁷T. Schedel-Niedrig, M. Hävecker, A. Knop-Gericke, and R. Schlögl, *Phys. Chem. Chem. Phys.* **2**, 3473 (2000).
- ⁴⁸S. Y. Lee, N. Mettlach, N. Nguyen, and J. M. W. Y. M. Sun, *Appl. Surf. Sci.* **206**, 102 (2003).
- ⁴⁹A. Soon, T. Sönnel, and H. Idriss, *Surf. Sci.* **579**, 131 (2005).
- ⁵⁰A. Martínez-Ruiz, M. G. Moreno, and N. Takeuchi, *Solid State Sci.* **5**, 291 (2003).
- ⁵¹E. Ruiz, S. Alvarez, P. Alemany, and R. A. Evarestov, *Phys. Rev. B* **56**, 7189 (1997).
- ⁵²W. G. Wickoff, *Crystal Structures* (Wiley-Interscience, New York, 1960), Vol. 1.
- ⁵³A. F. Wells, *Structural Inorganic Chemistry*, 5th ed. (Clarendon, Oxford, 1984).
- ⁵⁴A. Werner and H. D. Hochheimer, *Phys. Rev. B* **25**, 5929 (1982).
- ⁵⁵H. Werner, D. Herein, G. Schulz, U. Wild, and R. Schlögl, *Catal. Lett.* **49**, 109 (1997).
- ⁵⁶Q. Sun, K. Reuter, and M. Scheffler, *Phys. Rev. B* **67**, 205424 (2003).

- ⁵⁷M. V. Twigg and M. S. Spencer, *Top. Catal.* **22**, 191 (2003).
- ⁵⁸M. Todorova, Ph.D. thesis, Technical University Berlin, Berlin, 2004.
- ⁵⁹J. Gustafson, A. Mikkelsen, M. Borg, E. Lundgren, L. Köhler, G. Kresse, M. Schmid, P. Varga, J. Yuhara, X. Torrelles *et al.*, *Phys. Rev. Lett.* **92**, 126102 (2004).
- ⁶⁰L. Köhler, G. Kresse, M. Schmid, E. Lundgren, J. Gustafson, A. Mikkelsen, M. Borg, J. Yuhara, J. N. Andersen, M. Marsman, and P. Varga, *Phys. Rev. Lett.* **93**, 266103 (2004).
- ⁶¹J. Schnadt, A. Michaelides, J. Knudsen, R. T. Vang, K. Reuter, E. Laegsgaard, M. Scheffler, and F. Besenbacher, *Phys. Rev. Lett.* **96**, 146101 (2006).
- ⁶²M. Schmid, A. Reicho, A. Stierle, I. Costina, J. Klikovits, P. Kostelnik, O. Dubay, G. Kresse, J. Gustafson, E. Lundgren, J. N. Andersen, H. Dosch, and P. Varga, *Phys. Rev. Lett.* **96**, 146102 (2006).